

Chapter 5

Anisotropic star with Linear equation of state

A family of solutions defining the interior of a static, spherically symmetric, compact anisotropic star is described by considering a new form of the equation of state. The analytic solution is derived by using the Finch and Skea ansatz for the metric potential g_{rr} , which has a clear geometric interpretation for the related background spacetime. The model parameters are fixed by smooth matching of the interior solution to the Schwarzschild exterior metric over the bounding surface of the compact star, together with the requirement that the radial pressure vanishes at the boundary. Data available for the pulsar $4U1802030$ has been utilized to analyze physical viability of the developed model. The model is shown to be stable.

5.1 Introduction

Since the groundbreaking work of Schwarzschild, generating an exact solution for a spherically symmetric perfect fluid distribution in general relativity has been subject of extensive study. Solutions to Einstein's field equations for geometrically

meaningful spacetimes satisfying all the physical criteria are crucial in theoretical astrophysics. However, the non-linear nature of the Einstein field equations makes it difficult to find regular exact solutions fulfilling all the physical requirements. In addition, a feasible solution should also be able to describe realistic objects.

In the high density regime of compact stars, linearity of the equation of state of the matter composition appears to be a good approximation. Nilsson and Uggla [141] studied static spherically symmetric perfect fluid stellar models with a linear barotropic equation of state. Ivanov [80] investigated relativistic static fluid spheres assuming a linear equation of state. Maharaj and Chaisi [124] developed new class of exact interior solutions to Einstein field equations and analyzed its physical behaviour. Sharma and Maharaj [178] obtained new exact solution to Einstein field equations making use of a linear equation of state. New class of exact solutions to Einstein-Maxwell system was obtained by Thirukkanesh and Maharaj [189]. Maharaj and Thirukkanesh [126] also studied charged anisotropic matter distributions by assuming a linear equation of state. Varela *et al* [212] analyzed charged anisotropic star by considering linear as well as nonlinear equation of state. Maharaj *et al* [128] developed a model for a quark star by considering a linear equation of state. Ngubelanga *et al* [140] obtained solutions to field equations in isotropic coordinates. Harko and Mak [70] analyzed a power series solution for a stellar structure composed of an isotropic fluid which admits a linear barotropic or polytropic equation of state. Anisotropic compact stellar objects admitting a linear equation of state was studied by Banerjee [9]. Prasad and Jitendra [152] presented a class of relativistic solutions to Einstein field equations for an anisotropic matter distribution utilizing the Buchdahl ansatz for the metric function g_{rr} . Recently, Patel *et al* [155] investigated a charged anisotropic stellar solution in paraboloidal spacetime using a linear equation of state. All these studies are aimed at developing stellar models which are compatible with observational data.

While developing such models, one assumes a linear equation of state of the form $p_r = \alpha\rho - \beta$, where ρ is the density and p_r is the radial pressure and α and β are constants. Note that the linearity is in terms of density and not in terms of the radial variable r . This implies that α and β might not be constants and could be the functions of the radial variable r as well. Keeping this in mind in our work, to develop an anisotropic stellar model, we assume a linear equation of state of the form $p_r = \alpha \left(1 - \frac{r^2}{R^2}\right) \rho$, where $0 < \alpha < 1$. This assumption allows us to generate a new class of exact solution to the Einstein field equations which is physical plausible.

5.2 Field Equation

To develop the model of a static, spherically symmetric anisotropic star, we assume the spacetime metric in the form

$$ds^2 = e^{\nu(r)} dt^2 - e^{\lambda(r)} dr^2 - r^2(d\theta^2 + \sin^2\theta d\phi^2). \quad (5.1)$$

The energy-momentum tensor is assumed of the form

$$T_{ij} = (\rho + p_{\perp})u_i u_j + p g_{ij} + \pi_{ij}, \quad (5.2)$$

where ρ and p represent energy-density and isotropic pressure respectively and u_i is the unit 4-velocity of fluid. The anisotropic stress-tensor π_{ij} is assumed to be of the form

$$\pi_{ij} = \sqrt{3}S[C_i C_j - \frac{1}{3}(u_i u_j - g_{ij})], \quad (5.3)$$

where $S = S(r)$ denotes the magnitude of anisotropy and $C^i = (0, -e^{\frac{\lambda}{2}}, 0, 0)$ is a radially directed vector. We calculate the non-vanishing components of the energy-

momentum tensor as

$$T_0^0 = \rho, \quad T_1^1 = -\left(p + \frac{2S}{\sqrt{3}}\right), \quad T_2^2 = T_3^3 = -\left(p - \frac{S}{\sqrt{3}}\right), \quad (5.4)$$

and define the radial and tangential pressures as

$$p_r = p + \frac{2S}{\sqrt{3}}, \quad p_\perp = p - \frac{S}{\sqrt{3}}. \quad (5.5)$$

The magnitude of anisotropy obtained as

$$S = \frac{p_r - p_\perp}{\sqrt{3}}. \quad (5.6)$$

The Einstein field equations, for the spacetime metric (5.1), together with the energy momentum tensor (5.2), leads to the following independent equations

$$8\pi\rho = \frac{e^{-\lambda}\lambda'}{r} + \frac{1 - e^{-\lambda}}{r^2}, \quad (5.7)$$

$$8\pi p_r = \frac{e^{-\lambda}\nu'}{r} + \frac{e^{-\lambda} - 1}{r^2}, \quad (5.8)$$

$$8\pi p_\perp = e^{-\lambda} \left(\frac{\nu''}{2} + \frac{\nu'^2}{4} - \frac{\nu'\lambda'}{4} + \frac{\nu' - \lambda'}{2r} \right), \quad (5.9)$$

$$8\pi\sqrt{3}S = e^{-\lambda} \left(\frac{-\nu''}{2} - \frac{\nu'^2}{4} + \frac{\nu'}{2r} + \frac{1}{r^2} - \frac{e^\lambda}{r^2} + \frac{\lambda'}{2r} + \frac{\nu'\lambda'}{4} \right). \quad (5.10)$$

The technique to solve the system is discussed in the next section.

5.3 Technique to Generate New Stellar Solutions

We are presented with a system of three equations involving five unknowns

$(\rho, p_r, p_\perp, e^{\lambda(r)}, e^{\nu(r)})$. The system can be solved completely by choosing any two

unknowns from this collection; there are 10 possible combinations for these pairs.

In various studies, different pairs of variables have been chosen to model compact stars. Bhar *et al* [14], and Bhar and Ratanpal [15] opted for $e^{\lambda(r)}$ and p_r . Bhar and Rahaman [12] selected ρ and p_r . Thirukkanesh *et al* [193] considered $e^{\nu(r)}$ along with the measure of anisotropy. On the other hand, Sharma and Maharaj [178], Bhar *et al* [14], Sunzu *et al* [181], Komathiraj and Maharaj [88], Bhar [11], Bhar *et al* [18], Bhar *et al* [16], Das *et al* [39], Das *et al* [40], and Ratanpal and Patel [162] chose $e^{\lambda(r)}$ and the equation of state for their respective analyses. To develop a physically reasonable model of the stellar configuration, we assume the linear equation of state of the form

$$8\pi p_r = \alpha \left(1 - \frac{r^2}{R^2} \right) \rho, \quad (5.11)$$

where R is the radius of the star and $0 < \alpha < 1$. Equation (5.11) guarantees that the radial pressure is positive at the center and vanishes at the boundary of the star.

We further use the Finch and Skea ansatz for the metric potential g_{rr} as

$$e^{\lambda(r)} = 1 + \frac{r^2}{R^2}, \quad (5.12)$$

where R is the curvature parameter. The ansatz (5.12) has a geometric interpretation as can be found in reference [206].

Combining equations (5.8) and (5.11), we obtain

$$\nu' = r \left[e^{\lambda} \left(\alpha \rho \left(1 - \frac{r^2}{R^2} \right) + \frac{1}{r^2} \right) - \frac{1}{r^2} \right]. \quad (5.13)$$

Integration of (5.13) yields

$$e^{\nu} = CR^{4\alpha} \left(1 + \frac{r^2}{R^2} \right)^{2\alpha} \times \exp \left(\frac{(1-\alpha)\frac{r^2}{R^2}}{2} - \frac{\alpha\frac{r^4}{R^4}}{4} \right), \quad (5.14)$$

where C is a constant of integration. Thus, the interior spacetime metric takes the form

$$ds^2 = CR^{4\alpha} \left(1 + \frac{r^2}{R^2}\right)^{2\alpha} \times \exp\left(\frac{(1-\alpha)\frac{r^2}{R^2}}{2} - \frac{\alpha\frac{r^4}{R^4}}{4}\right) dt^2 - \left(1 + \frac{r^2}{R^2}\right) dr^2 - r^2(d\theta^2 + \sin^2\theta d\phi^2), \quad (5.15)$$

which is non-singular at $r = 0$.

Making use of Eqs. (5.11), (5.12), (5.13) and (5.14), the system of equations ((5.7)-(5.9)) reduces to

$$8\pi\rho = \frac{3 + \frac{r^2}{R^2}}{R^2\left(1 + \frac{r^2}{R^2}\right)^2}, \quad (5.16)$$

$$8\pi p_r = \frac{\alpha\left(1 - \frac{r^2}{R^2}\right)\left(3 + \frac{r^2}{R^2}\right)}{R^2\left(1 + \frac{r^2}{R^2}\right)^2}, \quad (5.17)$$

$$8\pi p_\perp =$$

$$\frac{12\alpha + \alpha^2\frac{r^{10}}{R^{10}} + 2\alpha(2\alpha - 1)\frac{r^8}{R^8} + (1 - 12\alpha - 2\alpha^2)\frac{r^6}{R^6} - 2(6\alpha^2 + 7\alpha - 2)\frac{r^4}{R^4} + (3 - 16\alpha + 9\alpha^2)\frac{r^2}{R^2}}{4R^2\left(1 + \frac{r^2}{R^2}\right)^3}, \quad (5.18)$$

$$8\pi\sqrt{3}S =$$

$$\frac{-\frac{r^2}{R^2}\left((3 - 20\alpha + 9\alpha^2) - 2\frac{r^2}{R^2}(6\alpha^2 + \alpha - 2) + \frac{r^4}{R^4}(1 - 8\alpha - 2\alpha^2) + 2\alpha\frac{r^6}{R^6}(2\alpha - 1) + \frac{r^8}{R^8}\alpha^2\right)}{4R^2\left(1 + \frac{r^2}{R^2}\right)^3}. \quad (5.19)$$

5.4 Exterior Spacetime and Boundary Conditions

The model has three independent parameters, namely, α , C , and R . Two of these constants can be evaluated by matching the interior spacetime metric (5.15) to the Schwarzschild exterior metric

$$ds^2 = \left(1 - \frac{2M}{r}\right) dt^2 - \left(1 - \frac{2M}{r}\right)^{-1} dr^2 - r^2(d\theta^2 + \sin^2\theta d\phi^2), \quad (5.20)$$

across the boundary $r = R$ of the star together with the condition that the radial pressure should vanish at the surface ($p_r(r = R) = 0$). The process fixes the constants as

$$C = \frac{\exp\left(\frac{3\alpha}{4} - \frac{1}{2}\right)}{2^{(2\alpha+1)} R^{4\alpha}}, \quad (5.21)$$

$$M = \frac{R}{4}, \quad (5.22)$$

The constant C depends on α , which remains as a free parameter.

5.5 Physical Conditions

For a physically acceptable stellar model, the following conditions should be satisfied (Finch and Skea [58], Delgaty and Lake [45]):

- (i) $\rho(r) \geq 0$, $p_r(r) \geq 0$, $p_{\perp}(r) \geq 0$, for $0 \leq r \leq R$.
- (ii) $\frac{d\rho}{dr} \leq 0$, $\frac{dp_r}{dr} \leq 0$, $\frac{dp_{\perp}}{dr} \leq 0$, for $0 \leq r \leq R$
- (iii) $0 \leq \frac{dp_r}{d\rho} \leq 1$, $0 \leq \frac{dp_{\perp}}{d\rho} \leq 1$, for $0 \leq r \leq R$
- (iv) $\rho - p_r - 2p_{\perp} \geq 0$, for $0 \leq r \leq R$
- (v) $\Gamma > \frac{4}{3}$, for $0 \leq r \leq R$.

Using graphical method, we demonstrate that all of the above mentioned conditions are satisfied in this model. The energy density in this model takes the form

$$8\pi\rho = \frac{3 + \frac{r^2}{R^2}}{R^2(1 + \frac{r^2}{R^2})^2}. \quad (5.23)$$

Thus, the central density takes the value

$$\rho(0) = \frac{3}{R^2}.$$

Obviously, we have $\rho_{r=0} > 0$ and $\rho_{r=R} > 0$. The gradient of density is obtained as

$$\frac{d\rho}{dr} = -\frac{2\frac{r}{R}\left(5 + \frac{r^2}{R^2}\right)}{R^3\left(r^2 + R^2\right)^3}, \quad (5.24)$$

it can be shown from equation (5.24) that the density is a decreasing function of r .

The condition ($\frac{d\rho}{dr}_{r=0} < 0$ and $\frac{d\rho}{dr}_{r=R} < 0$) puts the restriction on $0 < \alpha < 1$. The

radial pressure

$$8\pi p_r = \frac{\alpha\left(1 - \frac{r^2}{R^2}\right)\left(3 + \frac{r^2}{R^2}\right)}{R^2\left(1 + \frac{r^2}{R^2}\right)^2}, \quad (5.25)$$

calculated the centre takes the form

$$p_r(0) = \frac{3\alpha}{R^2}.$$

We note that the condition $p_r(r = 0) > 0$ and $p_r(r = R) > 0$ are satisfies if

$0 < \alpha < 1$. Differentiating (5.25) with respect to r , we obtain

$$\frac{dp_r}{dr} = -\frac{16\alpha\frac{r}{R}}{R^3\left(r^2 + R^2\right)^3}, \quad (5.26)$$

which is a decreasing function of r provided $0 < \alpha < \frac{1}{4}$. The tangential pressure p_\perp

has the form $8\pi p_\perp =$

$$\frac{12\alpha + \alpha^2\frac{r^{10}}{R^{10}} + 2\alpha(2\alpha - 1)\frac{r^8}{R^8} + (1 - 12\alpha - 2\alpha^2)\frac{r^6}{R^6} - 2(6\alpha^2 + 7\alpha - 2)\frac{r^4}{R^4} + (3 - 16\alpha + 9\alpha^2)\frac{r^2}{R^2}}{4R^2\left(1 + \frac{r^2}{R^2}\right)^3}, \quad (5.27)$$

and its central value is

$$p_\perp(0) = \frac{3\alpha}{R^2}.$$

Thus, $p_\perp(r = 0) > 0$. Also, the gradient of tangential pressure $\frac{dp_\perp}{dr} =$

$$\frac{\frac{r}{R}(9\alpha^2 - 52\alpha + 3) + 2(1 + 2\alpha - 21\alpha^2)\frac{r^3}{R^3} + (6\alpha^2 - 22\alpha - 1)\frac{r^5}{R^5} + 8\alpha\frac{r^7}{R^7} + \alpha(9\alpha - 2)\frac{r^9}{R^9} + 2\alpha^2\frac{r^{11}}{R^{11}}}{2R^3\left(r^2 + R^2\right)^4},$$

remains negative if $\alpha > \frac{1}{20}$. We also note that the radial pressure and tangential pressure are equal at the centre implying regularity of the anisotropic factor. Fig.(5.1) shows the variation of density inside the star which decreases radially outward. Fig.(5.2) and Fig.(5.3) show variations of the radial and tangential pressures respectively. The pressures are also decreasing functions of r . Fig.(5.6) shows the anisotropy which is a decreasing throughout the distribution.

Let us now check whether the bound on α also satisfies the causality condition $0 < \frac{dp_r}{d\rho} < 1$ and $0 < \frac{dp_\perp}{d\rho} < 1$. We have

$$\frac{dp_r}{d\rho} = \frac{8\alpha}{5 + \frac{r^2}{R^2}},$$

$$\frac{dp_\perp}{d\rho} =$$

$$\frac{\alpha(2 - 9\alpha)\frac{r^8}{R^8} + 8\alpha(1 - 2\alpha)\frac{r^6}{R^6} + (1 + 22\alpha - 6\alpha^2)\frac{r^4}{R^4} + 2(21\alpha^2 - 2\alpha - 1)\frac{r^2}{R^2} + (-3 + 52\alpha - 9\alpha^2)}{4(1 + \frac{r^2}{R^2})(5 + \frac{r^2}{R^2})},$$

The conditions $0 \leq \frac{dp_r}{d\rho} (r=0) \leq 1$ and $0 \leq \frac{dp_r}{d\rho} (r=R) \leq 1$ are evidently satisfied at the centre as well as at the boundary.

The condition $0 \leq \frac{dp_\perp}{d\rho} (r=0) \leq 1$ and $0 \leq \frac{dp_\perp}{d\rho} (r=R) \leq 1$ are evidently satisfied at the centre as well as at the boundary provided $\frac{1}{9}(26 - \sqrt{649}) < \alpha < \frac{1}{9}(26 + \sqrt{649})$ and $\frac{1}{20} < \alpha < \frac{13}{20}$. In Fig.(5.4) and Fig.(5.5), we show the variation of $\frac{dp_r}{d\rho}$ and $\frac{dp_\perp}{d\rho}$ against r . Both quantities satisfy the condition $0 < \frac{dp_r}{d\rho} < 1$ and $0 < \frac{dp_\perp}{d\rho} < 1$, indicating that the sound speed is less than the speed of light throughout the star. Table (5.3) shows the values of $\frac{dp_r}{d\rho}$ and $\frac{dp_\perp}{d\rho}$ at the center as well as the surface of the star.

5.5.1 Energy Conditions

Conditions (i) and (ii) imply fulfillment of the weak and dominant energy conditions.

Condition (iv) ensures regular behaviour of the energy density. Now, we have

$$(\rho - p_r - 2p_\perp)_{(r=0)} = \frac{3(1 - 3\alpha)}{R^2}, \quad (5.28)$$

and

$$(\rho - p_r - 2p_\perp)_{(r=R)} = \frac{4\alpha + 1}{2R^2}. \quad (5.29)$$

In order to examine fulfillment of the strong energy condition, we evaluate $\rho - p_r - 2p_\perp$ at the centre and at the boundary of the star. It is observed that the bound on $0 < \alpha < \frac{1}{3}$ fulfills this condition. Fig.(5.7) indicates that the strong energy condition $\rho - p_r - 2p_\perp > 0$ is satisfied throughout the distribution within the bound of α where we have used the data obtained for the pulsar $4U1820 - 30$. Table (5.1) shows the values of $\rho - p_r - 2p_\perp$ at the center as well as the surface of the star.

5.5.2 Stability

(i) Causality condition and method of cracking: The stability of a stellar structure is critical in relativistic astrophysics. The causality criterion states that a physically plausible model's radial sound velocity v_r^2 and tangential sound velocity v_\perp^2 must fall within the interval $[0, 1]$. The expressions for the radial v_r^2 and tangential v_\perp^2 velocities of sound are obtained as

$$v_r^2 = \frac{p'_r}{\rho'}, \quad v_\perp^2 = \frac{p'_\perp}{\rho'}, \quad (5.30)$$

$$(v_\perp^2 - v_r^2)_{(r=0)} = \frac{1}{20} (-9\alpha^2 + 20\alpha - 3), \quad (5.31)$$

$$(v_{\perp}^2 - v_r^2)_{(r=R)} = \frac{1}{12}(4\alpha - 1), \quad (5.32)$$

For $(v_{\perp}^2 - v_r^2)_{(r=0)} < 0$, we must have $(-9\alpha^2 + 20\alpha - 3) < 0$ i.e., $0 < \alpha < 0.161777$. At the boundary of the star, we have $(v_{\perp}^2 - v_r^2)_{(r=R)} < 0$. Thus, we must have $(4\alpha - 1) < 0$ i.e., $0 < \alpha < 0.240885$.

Herrera [73] introduced the concept of ‘‘cracking’’ to determine the stability of anisotropic matter distribution. Abreu *et al* [1] showed that the region for which $-1 \leq v_{\perp}^2 - v_r^2 \leq 0$ are potentially stable and the region for which $0 \leq v_{\perp}^2 - v_r^2 \leq 1$ are potentially unstable inside a stellar configuration. Ratanpal [161] analyzed the role of anisotropy in potentially stable or unstable regions based on the criteria put forward by Abreu. According to the theorem used by Ratanpal [161], if $8\pi\sqrt{3}S = p_r - p_{\perp}$ is a decreasing function of r , then the stellar configuration is potentially stable. Table (5.3) shows that numerical values of the $(v_{\perp}^2 - v_r^2)$ at center as well as boundary of the star for the compact object $4U1820 - 30$. Fig.(5.10) shows that $v_{\perp}^2 - v_r^2 < 0$. Thus, the solution is potentially stable within the following bound: $0 < \alpha < 0.161777$.

(ii) Adiabatic index:

Bondi [24] showed that a Newtonian isotropic sphere will be in equilibrium if the adiabatic index $(\Gamma) > 4/3$ which turns out to be true for a relativistic anisotropic fluid sphere as well. The adiabatic index Γ is given by

$$\begin{aligned} \Gamma_r &= \frac{\rho + p_r}{p_r} \frac{dp_r}{d\rho}, \\ &= \frac{8\alpha \frac{r^2}{R^2} - 8(\alpha + 1)}{\left(\frac{r^4}{R^r} + 4\frac{r^2}{R^2} - 5\right)}. \end{aligned} \quad (5.33)$$

Within the prescribed bound of α , the profile of the adiabatic index (Γ_r) is shown in Fig.(5.8). The plot shows that the radial adiabatic index profile is a monotonic

increasing function of r and that $\Gamma = \frac{\rho + p_r}{p_r} \frac{dp_r}{d\rho} > \frac{4}{3}$ everywhere inside the star thereby satisfying the stability requirement. Table 5.1 shows the value of Γ_r at the center of the star.

5.5.3 Gravitational Redshift

The redshift $z = \sqrt{1/e^\nu} - 1$ must be a decreasing function of r and finite for $0 \leq z \leq a$. For a relativistic star, it is expected that the redshift must decrease towards the boundary and be finite throughout the distribution. The value of redshift at origin is described in Table (5.1)

As above all the conditions are satisfied in the range of α is $0.06 < \alpha < 0.17$. Therefore, our model is stable in the region $0.06 < \alpha < 0.17$.

5.5.4 Stability under Three Different Forces

To assess the stability of the model, it is crucial to analyze the equilibrium state using the Tolman-Oppenheimer-Volkoff (TOV) equation. This stability equation, originally formulated by Tolman [208] and further developed by Oppenheimer and Volkoff [143], characterizes the internal structure of a spherically symmetric, static compact object that maintains equilibrium in the presence of anisotropy. The generalized form of the TOV equation serves to express the intricate balance within such a system

$$-\frac{(\rho + p_r)}{2} \nu' - \frac{dp_r}{dr} + \frac{2}{r}(p_\perp - p_r) = 0, \quad (5.34)$$

The TOV equation can be expressed in a simple form to describe the equilibrium condition by defining the forces as gravitational forces (F_g), hydrostatic forces (F_h)

and anisotropic forces (F_a). Thus,

$$F_g(r) + F_h(r) + F_a(r) = 0, \quad (5.35)$$

where,

$$F_g(r) = -\frac{1}{2} (\rho(r) + p_r(r)) \frac{d\nu}{dr}, \quad (5.36)$$

$$F_h(r) = -\frac{dp_r(r)}{dr}, \quad (5.37)$$

$$F_a(r) = \frac{2(p_\perp - p_r)}{r}. \quad (5.38)$$

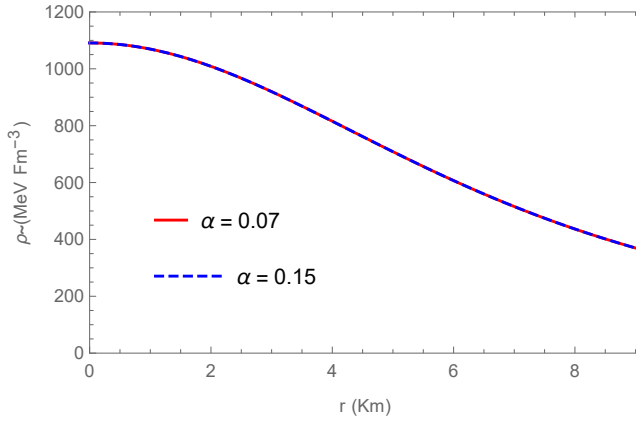
Hydrostatic and anisotropic forces work together to counteract gravitational force, maintaining equilibrium in the system.

Table 5.1: Fulfillment of the strong energy condition and values of the gravitational redshift at the center as well as at the surface and adiabatic index at the surface where we have used the data for the pulsar $4U1820 - 30$.

α	$\rho - \mathbf{p}_r - 2\mathbf{p}_\perp(r=0)$	$\rho - \mathbf{p}_r - 2\mathbf{p}_\perp(r=R)$	$\mathbf{Z}_{(r=0)}$ (Redshift)	$\mathbf{Z}_{(r=R)}$ (Redshift)	$\mathbf{\Gamma}_{(r=0)}$ (Adiabatic Index)
0.07	861.84	232.73	0.312942	0	1.71
0.08	829.114	240.007	0.317126	0	1.72
0.09	796.38	247.28	0.321323	0	1.74
0.10	763.65	254.55	0.325533	0	1.76
0.11	730.93	261.82	0.329757	0	1.77
0.12	698.201	269.09	0.333994	0	1.79
0.13	665.47	276.37	0.338245	0	1.8
0.14	632.74	283.644	0.342509	0	1.82
0.15	600.017	290.917	0.346787	0	1.84
0.16	567.28	298.19	0.351079	0	1.85

Table 5.2: Values of $\frac{d\rho}{dr}$, $\frac{dp_r}{dr}$ and $\frac{dp_\perp}{dr}$ at center as well as surface.

α	$\frac{d\rho}{dr}(r=0)$	$\frac{d\rho}{dr}(r=R)$	$\frac{dp_r}{dr}(r=0)$	$\frac{dp_r}{dr}(r=R)$	$\frac{dp_\perp}{dr}(r=0)$	$\frac{dp_\perp}{dr}(r=R)$
0.07	0	-59.94	0	-5.59	0	-1.99
0.08	0	-59.94	0	-6.39	0	-2.99
0.09	0	-59.94	0	-7.19	0	-3.99
0.10	0	-59.94	0	-7.99	0	-4.99
0.11	0	-59.94	0	-8.79	0	-5.99
0.12	0	-59.94	0	-9.59	0	-6.99
0.13	0	-59.94	0	-10.38	0	-7.99
0.14	0	-59.94	0	-11.18	0	-8.99
0.15	0	-59.94	0	-11.98	0	-9.99
0.16	0	-59.94	0	-12.78	0	-10.98

Figure 5.1: Variation of density against radial variable r .

5.6 Discussion

In the present work, we solved Einstein's field equations defining a spherically symmetric anisotropic matter by assuming the Finch and Skea ansatz and considering a linear equation of state of the form $p_r = \alpha \left(1 - \frac{r^2}{R^2}\right) \rho$, where $0 < \alpha < 1$. Physical grounds have been used to get bounds on the model parameters, and it has been demonstrated that the model is stable for $0.06 < \alpha < 0.17$. All the physical quantities are regular and well-behaved throughout the stellar interior for the star 4U1820-30 with radius $R = 9.1$ km and mass $M = 1.58M_\odot$. In Fig.(5.1),

Table 5.3: Values of $\frac{dp_r}{d\rho}$ and $\frac{dp_\perp}{d\rho}$ at the center as well as at the surface and at center.

α	$\frac{dp_r}{d\rho} (r=0)$	$\frac{dp_\perp}{d\rho} (r=0)$	$\frac{dp_r}{d\rho} (r=R)$	$\frac{dp_\perp}{d\rho} (r=R)$	$(\nu_t^2 - \nu_r^2)_{(r=0)}$	$(\nu_t^2 - \nu_r^2)_{(r=R)}$
0.07	0.112	0.029	0.093	0.033	-0.082	-0.06
0.08	0.128	0.055	0.106	0.055	-0.072	-0.056
0.09	0.144	0.08	0.12	0.066	-0.063	-0.053
0.10	0.16	0.105	0.13	0.083	-0.054	-0.05
0.11	0.176	0.130	0.146	0.1	-0.045	-0.046
0.12	0.192	0.15	0.16	0.11	-0.036	-0.043
0.13	0.208	0.180	0.173	0.133	-0.027	-0.04
0.14	0.224	0.205	0.186	0.15	-0.018	-0.036
0.15	0.24	0.229	0.2	0.16	-0.010	-0.033
0.16	0.256	0.254	0.213	0.183	-0.0015	-0.03

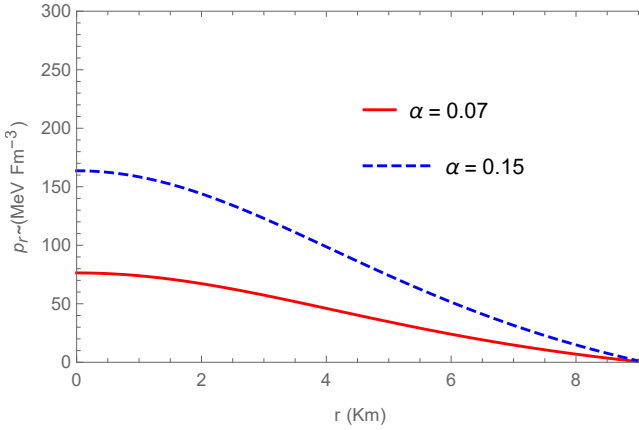
Figure 5.2: Variation of radial pressures against radial variable r .

Fig.(5.2) and Fig.(5.3), we examine the physical matter variables ρ , p_r , p_\perp graphically. Fig.(5.4) and Fig.(5.5) shows both the radial and tangential square of sound speed. In addition, the anisotropy for the model is shown to decreasing, as seen in Fig.(5.6). The energy criterion is met within the stellar structure. Since positive density and pressure are bound to be ≥ 0 , we investigate the profile of the SEC ($\rho - p_r - 2p_\perp$) graphically to confirm the stability in Fig.(5.7), and it is found to be satisfied for our model. We examined the adiabatic index, which is greater than $\frac{4}{3}$ across the structure (see Fig.(5.8)). It can be seen that the redshift maximizes at

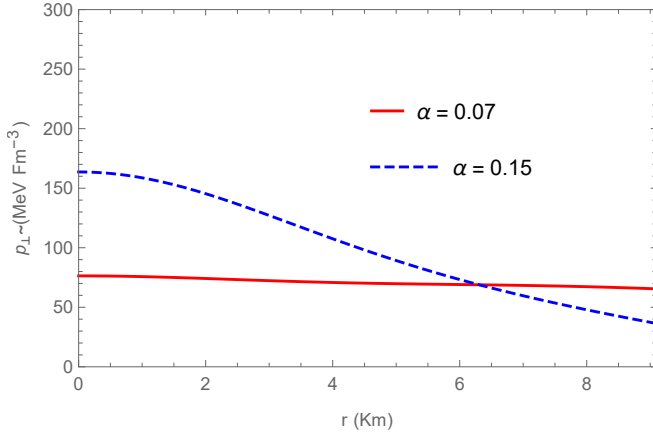


Figure 5.3: Variation of tangential pressures against radial variable r

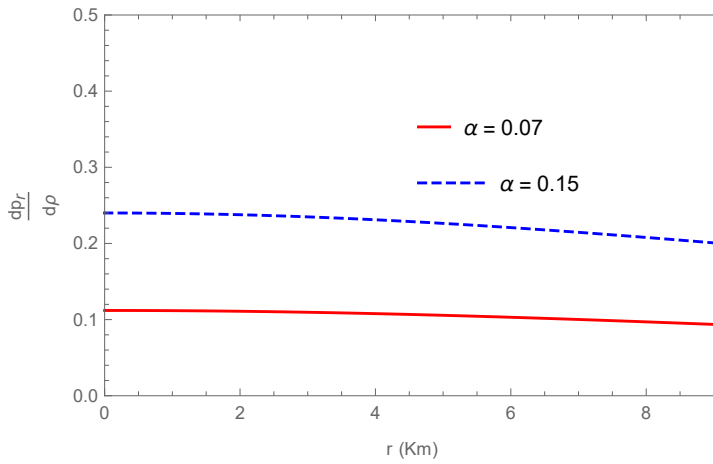


Figure 5.4: Variation of $\frac{dp_r}{d\rho}$ against radial variable r .

the centre shown in Fig.(5.9). Fig.(5.10) shows that $v_{\perp}^2 - v_r^2 < 0$ throughout the star. Fig.(5.11) and Fig.(5.12) shows the graphical representation of three distinct forces for the $\alpha = 0.07$ and $\alpha = 0.15$. We have shown that the model admits an equation of state which is linear in nature which is shown with graphical representation in Fig.(5.13). So the presented model satisfies all the physical criteria of a physically well-behaved compact object in the region $0.06 < \alpha < 0.17$.

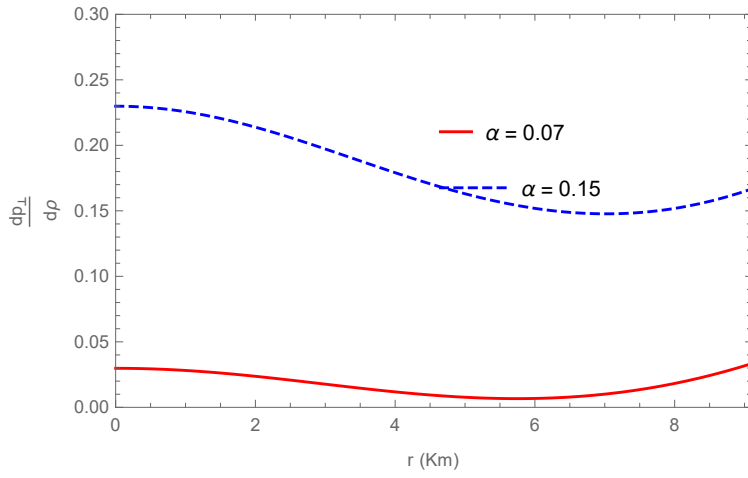


Figure 5.5: Variation of $\frac{dp_{\perp}}{d\rho}$ against radial variable r .

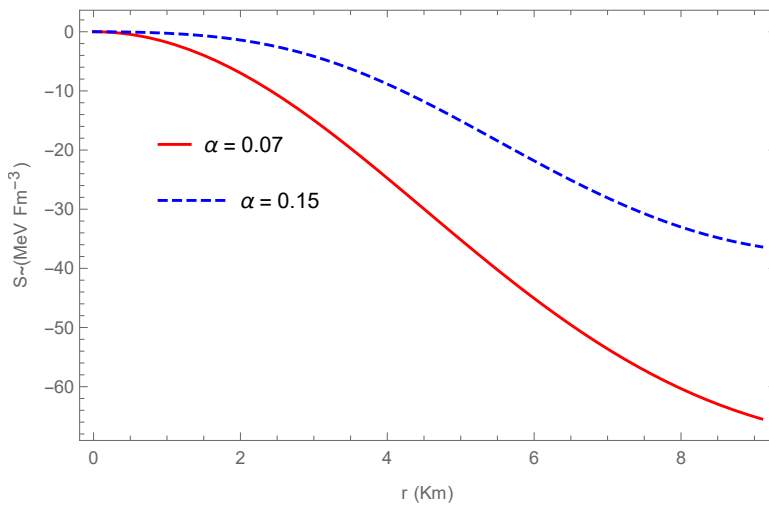


Figure 5.6: Variation of anisotropy against radial variable r .

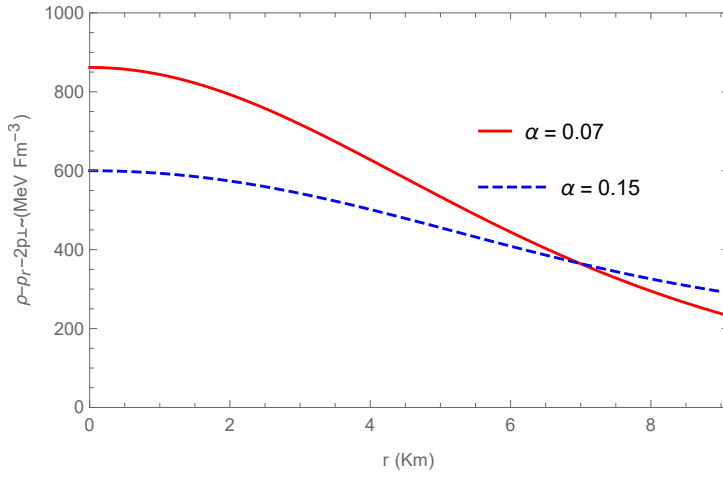


Figure 5.7: Variation of strong energy condition against radial variable r .

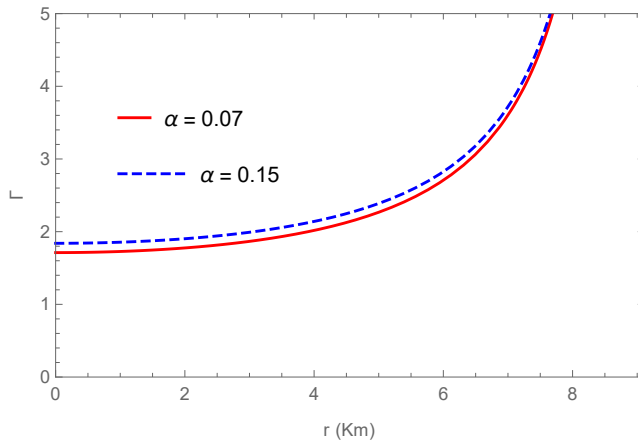


Figure 5.8: Variation of adiabatic Index against radial variable r .

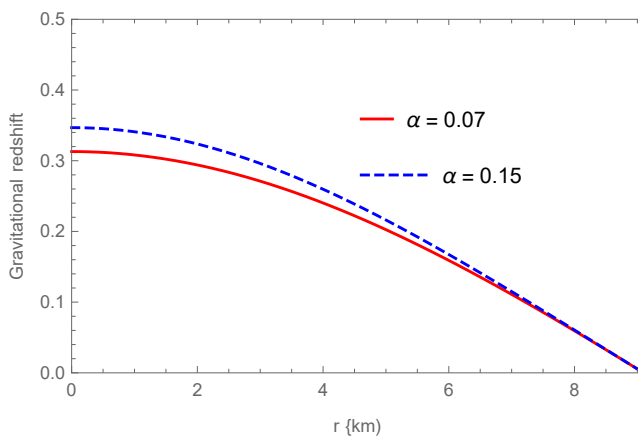


Figure 5.9: Variation of gravitational redshift against radial variable r .

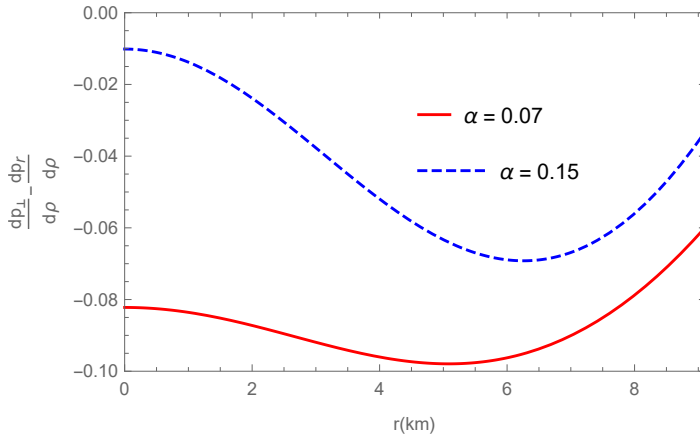


Figure 5.10: Variation of a stability expression $(\frac{dp_{\perp}}{d\rho} - \frac{dp_r}{d\rho})$ with respect to a radial coordinate r .

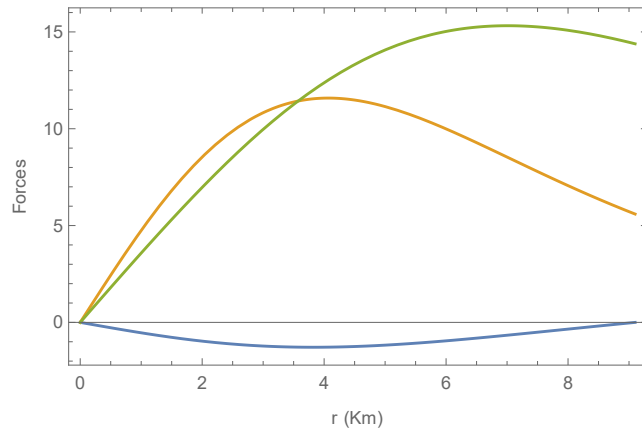


Figure 5.11: Variation of three forces like Gravitational Force(Blue), Hydrostatic Force(Orange) and Anisotropic Force(Green) for the value $\alpha = 0.07$.

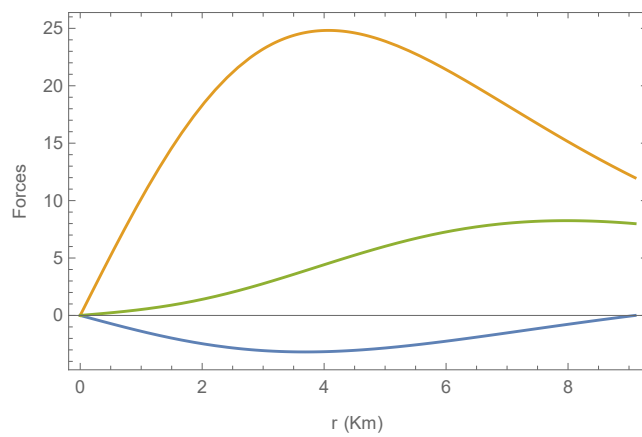


Figure 5.12: Variation of three forces like Gravitational Force(Blue), Hydrostatic Force(Orange) and Anisotropic Force(Green) for the value $\alpha = 0.15$.

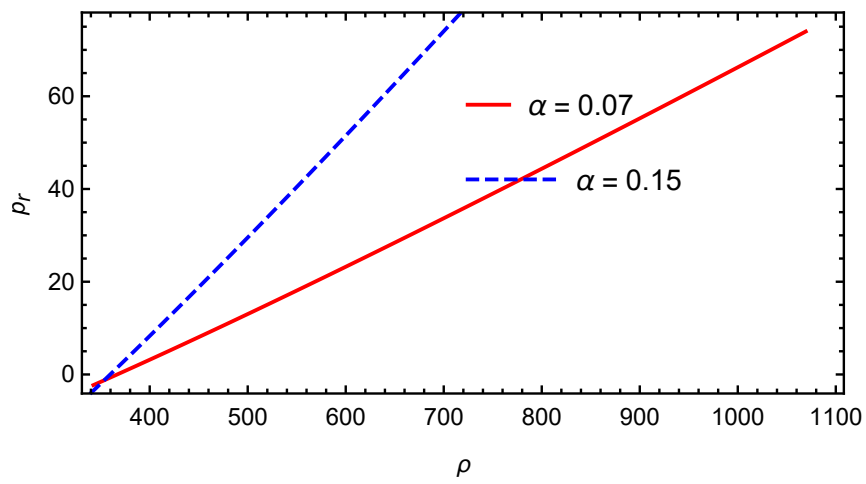


Figure 5.13: The relation between the pressure p_r and density ρ is plotted for the compact star